energies

MDPI

Article

Detection of Partial Demagnetization Faults in Five-Phase Permanent Magnet Assisted Synchronous Reluctance Machines

Carlos Candelo-Zuluaga, Jordi-Roger Riba *, Dinesh V. Thangamuthu and Antoni Garcia

Electrical Engineering Department, Universitat Politècnica de Catalunya, 08222 Terrassa, Spain; carlos.andres.candelo@upc.edu (C.C.-Z.); dineshthangamuthu1600@gmail.com (D.V.T.); garciae@ee.upc.edu (A.G.)

* Correspondence: riba@ee.upc.edu; Tel.: +34-937398365

Received: 16 June 2020; Accepted: 3 July 2020; Published: 6 July 2020

Abstract: This paper analyzes partial demagnetization faults in a five-phase permanent magnet assisted synchronous reluctance motor (fPMa-SynRM) incorporating ferrite permanent magnets (PMs). These faults are relevant because of the application of field weakening, or due to high operating temperatures or short circuit currents, the PMs can become irreversibly demagnetized, thus affecting the performance and safe operation of the machine. This paper proposes fault indicators to detect such fault modes with low demagnetization levels between 5.0% to 16.7% relative demagnetization. Four partial demagnetization fault detection methods are tested, which are based on the analysis of the harmonic content of the electromotive force (EMF) under no load conditions, the harmonic content of the line currents, the harmonic content of the zero-sequence voltage component (ZSVC) and the analysis of the power factor (PF). This work also compares the sensitivity and performance of the proposed detection methods. According to the fault indicators proposed in this paper, the results show that the analysis of the EMF, ZSVC and PF are the most sensitive detection methods. Experimental results are presented to validate finite element analysis (FEA) simulations.

Keywords: electric machines design; multi-phase motors; permanent magnet motors; synchronous reluctance motors; fault diagnosis; partial demagnetization faults; finite element analysis

1. Introduction

Synchronous reluctance machines (SynRMs) offer appealing characteristics, such as competitive cost, high overload capability and robustness [1]. However, SynRMs exhibit lower torque and power densities as well as lower power factor compared to permanent magnet synchronous machines (PMSMs). By inserting permanent magnets (PMs) in the flux barriers sculpted in the rotor, such weaknesses can be minimized, thus, resulting in a permanent magnet assisted SynRM (PMa-SynRM) [1]. PMa-SynRMs exhibit high torque and power density because the extra reluctance torque component [2] adds up to the alignment torque; these characteristics are interesting for automotive applications [3].

Rotating electric machines including rare-earth PMs present interesting characteristics, such as high torque/power density or improved efficiency [2], and wide speed range in the constant power region [3]. However, concerns such as rare-earth PMs price volatility or risk supply [4], machine manufacturers are developing machines with less content of rare-earth materials or even rare-earth-free. One alternative is to use ferrite PM, and thus, the machine is known as five-phase permanent magnet assisted synchronous reluctance motor (fPMa-SynRM). Ferrite PMs are economical compared to rare-earth PMs, but their remnant flux density is only about one-third of that of neodymium magnets [5]. Torque capability can be optimized by balancing design aspects related to saliency and permanent magnet utilization [6].

It is an accepted fact that since the main contribution of the total torque is the reluctance component, fPMa-SynRMs require lower PM volume than interior-PM motors (IPMs) [7].

In order to achieve high power or torque densities and to be resistant against demagnetization faults, a minimum volume or quantity of PMs must be inserted in the rotor. However, low PM content could only marginally increase the torque production, due to the low PM torque contribution compared to the total torque [1]. Under some circumstances, such as the application of field weakening, or the effects of high temperatures, high vibration levels or short circuit currents, fPMa-SynRMs can become irreversibly demagnetized, thus affecting their performance and safe operation. According to [8], fPMa-SynRMs can be easily demagnetized, particularly at lower temperatures, and thus, to minimize demagnetization risk, designs must consider limited electric loading and the flux barriers must be designed appropriately.

Therefore, it is crucial to detect PM demagnetization in the early stage to ensure that the machine runs under stable and safe conditions [9]. Early detection of demagnetization faults allows guiding maintenance plans, extending service life, minimizing unexpected shutdowns [10] and associated economic loss, while improving system reliability and availability [11]. Therefore, there is an imperious need to develop accurate diagnosis methods to detect incipient faults in critical applications where PMa-SynRMs play a pivotal role, such as in the automotive sector.

Fault diagnosis techniques can be broadly classified as off-line and on-line. Whereas the former methods are based on disconnecting the machine from the mains, the latter approach is most straightforward and simple to apply [12], since it does not require to disconnect the machine, although in some cases, specific sensors must be added to detect the faults. Faults can be detected on-line by monitoring and analyzing the voltages and currents at the machine terminals, although other magnitudes can be analyzed, including changes in the magnetic field, the input impedance, the vibrations pattern [13] or in the speed [14].

Motor current signature analysis (MCSA) comprehends a set of widespread methods for noninvasive and on-line fault detection and diagnosis of rotating electrical machines [15], including induction motors [16], SynRMs [17] or PMa-SynRMs [13], which are based on analyzing the stator currents pattern [18,19]. MCSA methods focus on measuring and monitoring the line currents of the rotating machine, which are post processed via the fast Fourier transform (FFT) or other related algorithms, to extract the spectral content under steady-state or quasi-steady-state operation. It is a recognized fact that any change in the machine, such as a fault condition, is reflected in the individual harmonics of the line currents [13]. The sensitivity of MCSA-based methods and the specific harmonic frequencies to be analyzed often depends on the topology of the analyzed rotating machine [20] and the operating conditions [13,21]. However, false indications could occur [22], since the speed drive current loop can alter the amplitude of the line currents harmonics [20].

It is known that demagnetization faults can be detected by studying the zero-sequence voltage component (ZSVC) spectrum [21,23]. The ZSVC is decoupled from the effects of the speed drive, at the expense of requiring an accessible neutral point of the wye stator windings [20]. In case of PM rotating machines, the analysis of the ZSVC tends to be more sensitive compared to the MCSA method based on the analysis of the line currents [20,24].

Another possibility to detect partial demagnetization faults is through the analysis of the power factor (PF), since due to the PMs, PMa-SynRMs present higher PF compared to SynRMs, thus reducing the inverter size. Therefore, this work assumes that demagnetization faults tend to reduce the PF of the PMa-SynRM. According to [25], the power factor of SynRMs can be written in terms of the d-axis and q-axis inductances, L_d and L_q, respectively:

$$\mathrm{PF} = (L_d/L_q - 1)/(L_d/L_q + 1) \tag{1}$$

From (1) it can be seen that a large value of the L_d/L_q saliency ratio allows maximizing the power factor. Different strategies can be applied for this purpose, including transversally and axially laminated rotor designs, by using suitable flux barriers in transversally laminated rotors or by inserting

permanent magnets into the flux barriers oriented along the q-axis opposing the flux of the stator, thus reducing the quadrature inductance L_q [25], while maximizing the L_d/L_q ratio.

Electric machines are designed to maximize performance, thus, they exhibit electrical and mechanical symmetry, which is often lost when operating under fault conditions. The loss of symmetry can be reflected in specific patterns in the waveform of different variables such as the stator currents, the electromotive force or vibrations [26]; thus, these patterns are useful for fault diagnosis. Contrasting with partial demagnetization faults, uniform demagnetization does not produce any asymmetric behavior of the machine [14], and thus, no new patterns or harmonic components arise in the waveforms [27]. Therefore, partial demagnetization faults could be detected by analyzing the change in the back-EMF under no load conditions, the PF of the machine under motoring operation or the change in the amplitudes of certain harmonic components of the stator currents or the zero-sequence voltage component (ZSVC).

This work is intended to detect partial demagnetization faults in fPMa-SynRMs. Different on-line methods are analyzed, including the analysis of the stator/line currents spectra, the analysis of the ZSVC spectrum, the study of the harmonic content of the back-EMF and the change of the PF. In addition, different demagnetization levels are studied by means of finite element analysis (FEA), since it is a widely recognized method to analyze in detail the behavior of electric machines [24].

At the best of the authors' knowledge, there are no papers dealing with demagnetization faults in PMa-SynRMs, thus, this paper contributes in this area, which also considers a multi-phase machine. Compared to other technologies, such as PMSMs, early demagnetization faults are more difficult to detect in fPMa-SynRMs, due to the lower impact of the permanent magnets on the overall performance of the machine, thus, this is a challenging problem. This area is generating a great interest, since in applications such as electromobility, early fault detection and fault diagnosis is a trending topic. This work discusses the advantages and drawbacks of the different studied fault detection methods and studies the particular operating conditions which ease the detection of such incipient faults. This paper also develops very fast fault indicators for an early detection of demagnetization faults in fPMa-SynRMs.

This paper is structured as described in the following lines. Section 2 describes the geometry, materials and main features of the analyzed machine, and develops and validates the corresponding FEA model. Section 3 describes the analyzed partial demagnetization faults. Section 4 summarizes the results obtained with the simulation model. Section 5 proposes fault indicators for detecting incipient partial demagnetization faults, and finally, Section 6 summarizes the conclusions of this work.

2. The Five-Phase Ferrite-Assisted fPMa-SynRM and Validation of the FEA Model

This section describes the geometry and the main features of the fPMa-SynRM analyzed in this paper and the FEA model developed to simulate the behavior of the machine when operating under healthy conditions and partial demagnetization faults. Although FEA is an internationally recognized numerical method for modeling rotating electric machines, the model used in this work has been validated from experimental data to prove its accuracy. Therefore, this section compares FEA simulation results against experimental measurements.

2.1. The fPMa-SynRM

Figure 1 displays the geometry of the analyzed machine.

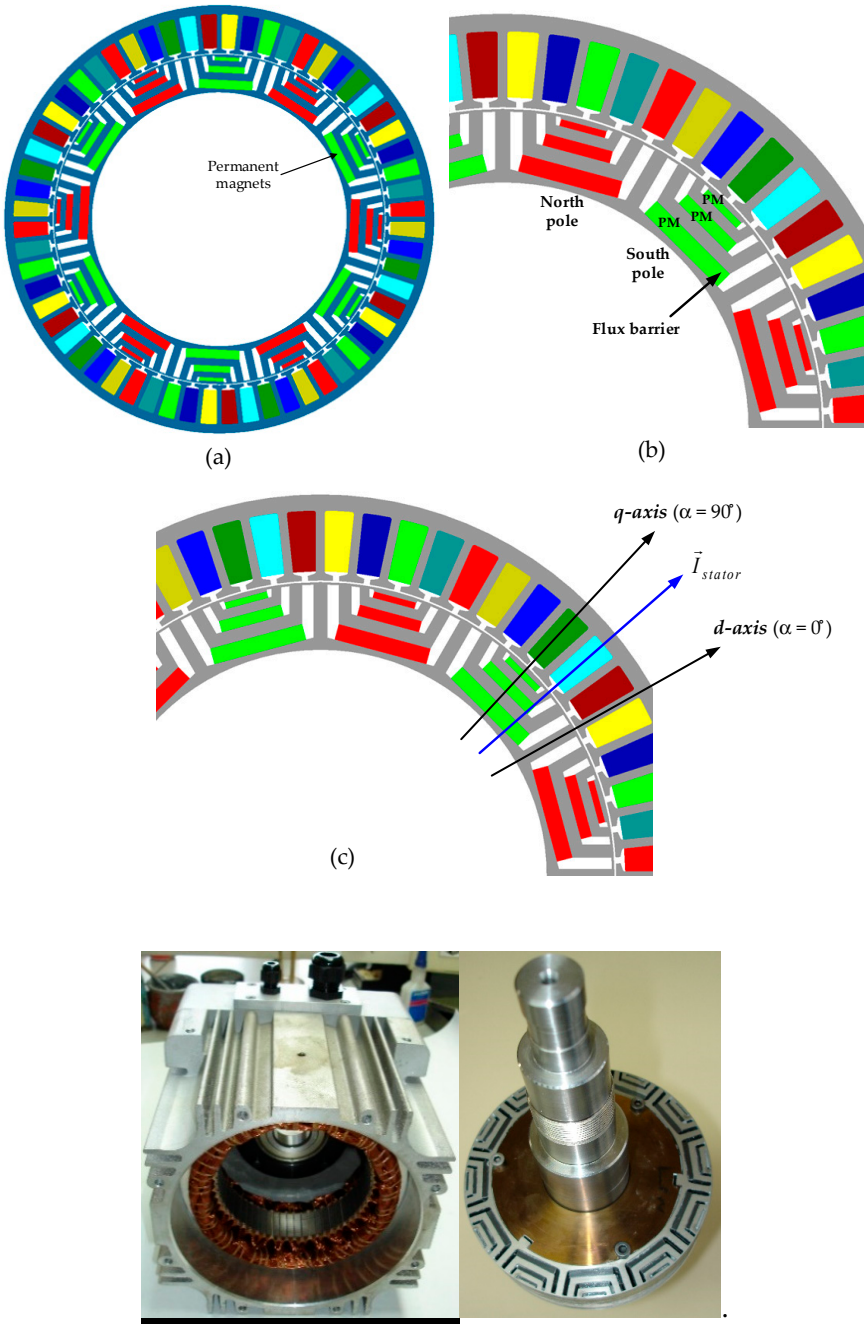

Figure 1. Layout of the analyzed five-phase permanent magnet assisted synchronous reluctance motor (fPMa-SynRM). (**a**) Stator and rotor arrangements. (**b**) Detail of the stator and rotor arrangements. (**c**) Stator current components (*d*- and *q*-axis). (**d**) Stator and rotor of the analyzed fPMa-SynRM.

As shown in Figure 1, the *q*-axis or quadrature axis is that directed towards the minimum flux, i.e., the direction crossing perpendicularly to the flux barriers. The *d*-axis or direct axis is directed towards the maximum magnetic flux, i.e., the magnetic flux direction following the magnetic path. As explained, the PMs are placed inside the flux barriers of the rotor, so that the PMs magnetization opposes to the direction of the *q*-axis, in order to maximize the L_d/L_q saliency ratio.

The main features of the analyzed fPMa-SynRM are summarized in Table 1.

Table 1. Main features of the analyzed fPMa-SynRM.

Characteristics	Value
Phase number	5
Nominal power (kW)	3.5
Nominal voltage (V_{RMS})	240
Nominal current (A_{RMS})	4
Nominal torque (N·m)	5.7
Nominal speed (rev/min)	5000
Alignment torque/total torque *	43.14%
Reluctant torque/total torque *	56.86%
Pole pairs (p)	6
External stator diameter (mm)	162.8
External rotor diameter (mm)	114
Laminations length (mm)	26
Air gap (mm)	0.3
Slots number	60
Conductors/slot	60
Slots per pole and per phase (q)	1
Winding type	Double layer
Permanent magnets material	Ferrite HF 30/26
Steel laminations	M330-35A
L_d (mH)	15.9 under maximum current ($i_d = i_{line,max,peak,1}$ **, $i_q = 0$) 59.7 under no current ($i_d = i_q = 0$)
L_q (mH)	11.8 under maximum current ($i_d = 0$, $i_q = i_{line,max,peak,1}$ **) 15.2 under no current ($i_d = i_q = 0$)

* At the optimal current angle ∈ (0°,90°), obtained as = arctg(i_q/i_d), and nominal value of the current. ** $i_{line,max,peak,1}$ refers to the maximum peak value of the fundamental harmonic of the line current.

Figure 2 depicts the magnetization curve of the ferrite PMs used in the analyzed fPMa-SynRM. It shows that the demagnetization curve behaves linearly until the knee point, and beyond this point, it drops abruptly. When the operating point is placed beyond the knee point, the permanent magnet never returns to its initial magnetic state [27].

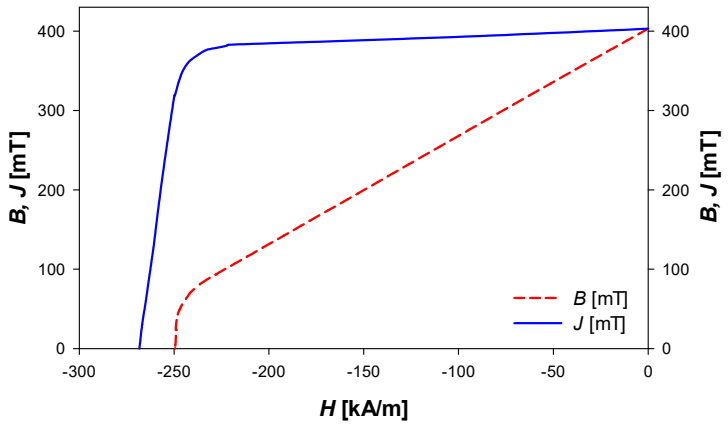

Figure 2. Demagnetization curve of the ferrite HF 30/26 permanent magnet material at 20 °C. Adapted from [28]. Magnetic polarization J and magnetic flux density B versus the magnetic field H, where $B = J + \mu_0 \cdot H$. Table 2 shows the main parameters of the finite element analysis (FEA) model generated in this work by means of the *Altair Flux*^{TM} FEA software.

Table 2. Harmonic content of the EMF in open circuit conditions underrated speed. Healthy and partially demagnetized fPMa-SynRMs.

Harmonic Order	1	2	3	4	5	6	7	8	9
Case 1. One magnetic pole 100% demagnetized									
Healthy (V)	**121.30**	-	**17.91**	-	0.76	-	5.35	-	**16.67**
Demagnetized (V)	**114.30**	-	**16.73**	-	0.56	-	4.63	-	**14.92**
Case 2. Two adjacent north magnetic poles 50% demagnetized									
Healthy (V)	**121.30**	-	**17.91**	-	0.76	-	**5.35**	-	**16.67**
Demagnetized (V)	**111.20**	1.57×10^{-3}	**16.68**	2.38×10^{-3}	9.76×10^{-3}	2.24×10^{-3}	**3.95**	2.65×10^{-3}	**13.35**
Case 3. Two adjacent north-south magnetic poles 50% demagnetized									
Healthy (V)	**121.30**	-	**17.91**	-	0.76	-	5.35	-	**16.67**
Demagnetized (V)	**108.10**	2.51×10^{-3}	**16.24**	2.88×10^{-3}	0.44	2.25×10^{-3}	4.83	2.27×10^{-3}	**14.61**
Case 4. Two adjacent north magnetic poles 100% demagnetized									
Healthy (V)	**121.30**	-	**17.91**	-	0.76	-	5.35	-	**16.67**
Demagnetized (V)	**107.50**	1.15×10^{-3}	**15.52**	8.69×10^{-4}	0.38	6.29×10^{-4}	3.88	5.58×10^{-4}	**13.29**
Case 5. Two adjacent north-south magnetic poles 100% demagnetized									
Healthy (V)	**121.30**	-	**17.91**	-	0.76	-	5.35	-	**16.67**
Demagnetized (V)	**101.80**	4.29×10^{-4}	**15.01**	5.23×10^{-4}	0.57	3.42×10^{-4}	4.51	4.22×10^{-4}	**13.67**
Case 6. Two magnets of the same pole 100% demagnetized									
Healthy (V)	**121.30**	-	**17.91**	-	0.76	-	5.35	-	**16.67**
Demagnetized (V)	**114.9**	-	**16.85**	-	0.64		4.71		**15.11**
Case 7. One magnet 100% demagnetized									
Healthy (V)	**121.30**	-	**17.91**	-	0.76	-	5.35	-	**16.67**
Demagnetized (V)	**116.50**	-	**17.02**	-	0.72	-	4.82	-	**15.40**

* Bold numbers indicate the most discriminating harmonics.

2.2. The FEA Model of the fPMa-SynRM

A full FEA model of the fPMa-SynRM was developed by means of the *Altair Flux*^{TM} FEA software, which is shown in Figure 3.

Magnetic transient simulations were carried out to simulate the machine operating under healthy and partial demagnetization conditions. The air gap was simulated taking into account three layers, i.e., a rotating air layer which is in contact with the rotor surface, an intermediate compressible layer and a fixed layer in contact with the inner stator surface, as shown in Figure 3b.

To represent the external flux leakage out of the stator in the FEA model, an infinite domain composed of two main layers was created. The inner infinite layer includes the Neumann's boundary condition, which ensures the flux continuity between the air and the infinite domain. The outer infinite layer includes the Dirichlet's boundary condition. The rest of boundaries include the Neumann's boundary condition.

The mechanical components are divided in two main groups, i.e., the rotating components belonging to the rotor (permanent magnets, shaft, rotor lamination part, inner rotor air and the rotating air gap layer) and the static components belonging to the stator (static air-gap layer, windings, stator laminations, air included within the stator slots and the external air-gap with the infinite domain included). Finally, an independent mechanical group is set to include the intermediate air-gap layer, which is re-meshed after each time step, to ensure the correct stator-rotor coupling.

2.3. The Validation of the FEA Model

The fPMa-SynRM was tested in the facilities of the Universitat Politècnica de Catalunya under open circuit conditions, as a generator, running at a constant speed of 2000 rev/min, impulsed by means of a secondary surface-mounted permanent magnet synchronous machine (1FT6108-8SB71-1DK3 from Siemens) acting as a motor.

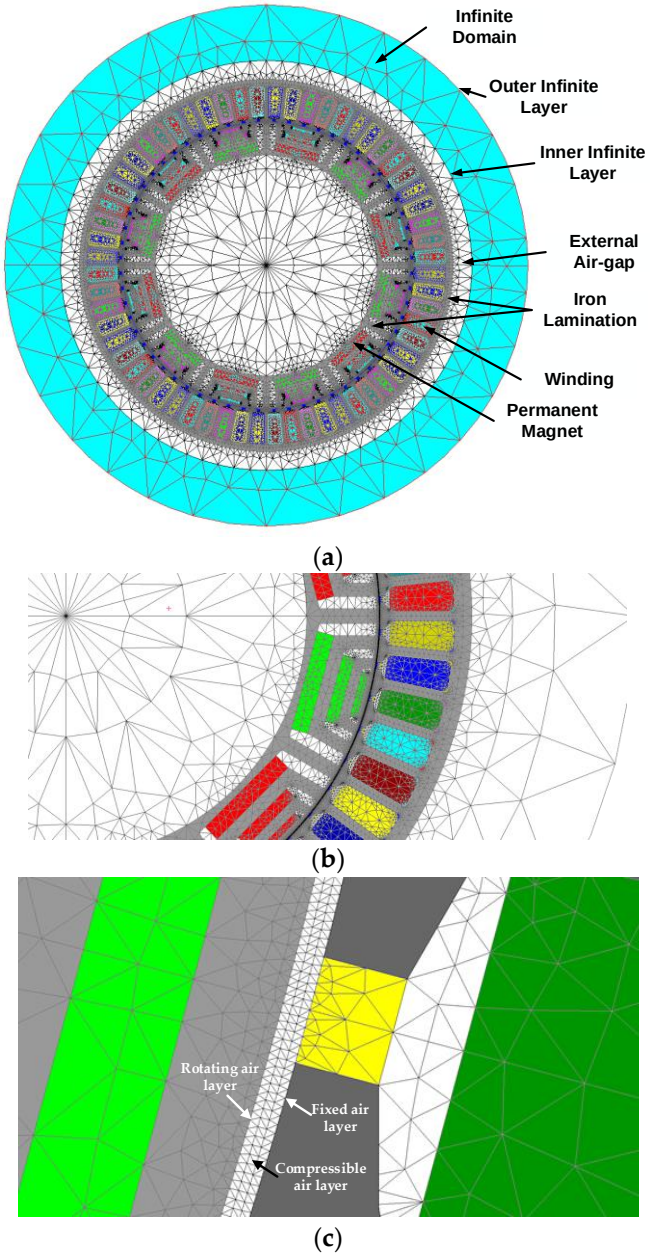

Figure 3. (**a**) The mesh of the full machine. The mesh includes about 152,000 nodes, 25,000 line elements and 75,000 surface elements. (**b**) Detail of the mesh. (**c**) Detail of the slot opening and the three layers to model the air gap.

The experimental EMF was acquired by means of a digital oscilloscope (Tektronix MDO3024 200 MHz 2.5 GS/s; Tektronix, Beaverton, OR, USA) connected to different voltage probes (Tektronix TPP0250 250 MHz; Tektronix, Beaverton, OR, USA). The test bench (see Figure 4b) includes a torque sensor (T22 from HBM), encoders (RI76TD from Hengstler), the PMSM acting as a motor, a CompactRIO data acquisition system and two frequency converters (Siemens Sinamics cp-320).

Figure 4 compares experimental results of the studied fPMa-SynRM with those obtained by means of FEA simulations using the model detailed in Section 2.2.

Results presented in Figure 4 show a close agreement between experimental and simulated results, thus validating the FEA model. However, the real machine always presents small asymmetries due to different effects, such as rotor unbalance and eccentricity, slight differences among the magnetization of the permanent magnets, or small asymmetries due to end coils effects, among others.

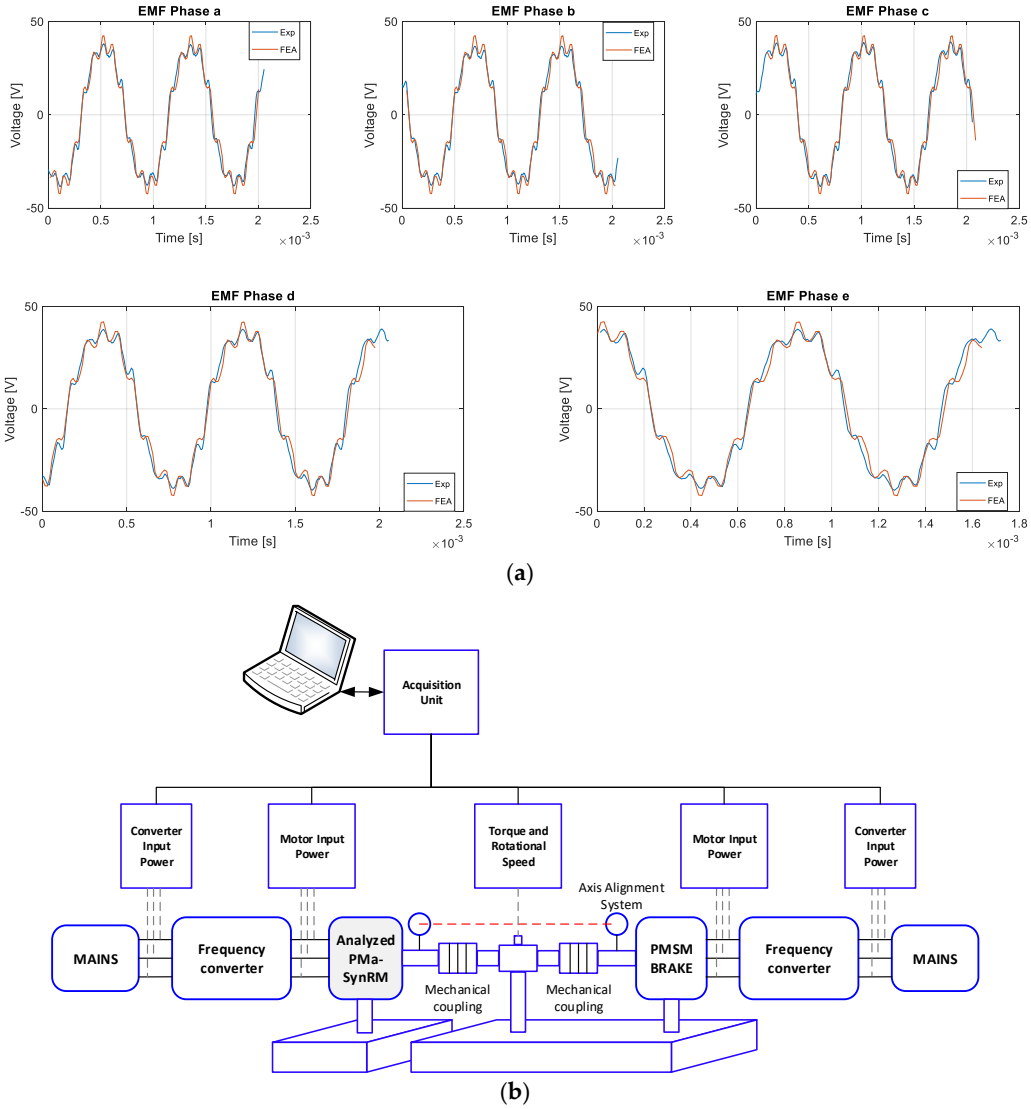

Figure 4. (**a**) Measured and experimental electromotive force (EMF) of the fPMa-SynRM operating at a constant speed of 2000 rev/min under healthy conditions. (**b**) Schematics of the test bench.

3. Analyzed Partial Demagnetization Faults

This section studies different partial demagnetization cases since it is believed that the type of demagnetization can impact the sensitivity of the fault detection methods, i.e., the analysis of the EMF under open circuit conditions, and the analysis of the stator currents harmonics, the analysis of the harmonic content of the ZSVC and the study of the power factor underrated speed and applying the maximum i_d current ($i_q = 0$). To this end, five partial demagnetization cases are analyzed, which are listed below and displayed in Figure 5.

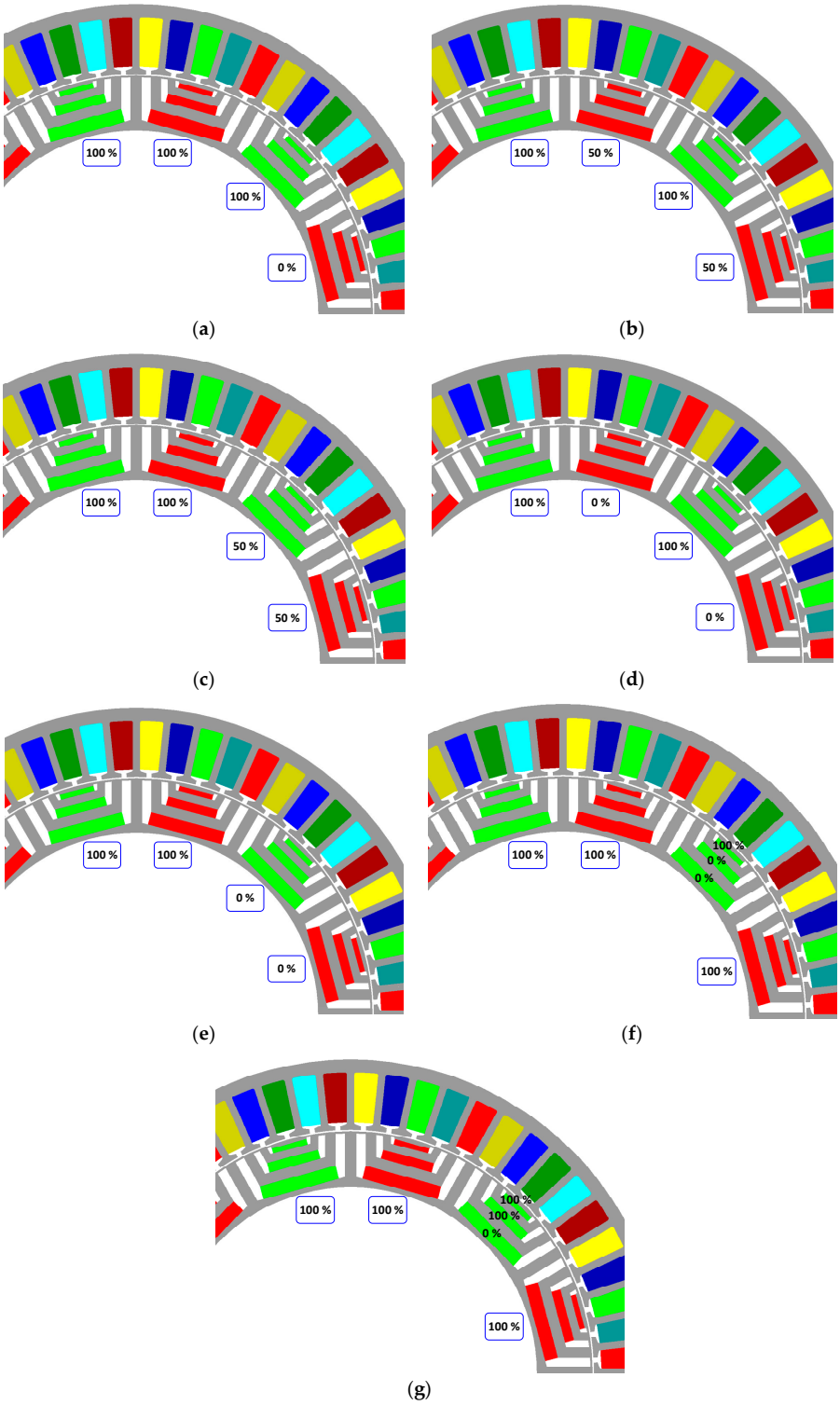

Figure 5. Different analyzed demagnetization faults underrated speed and applying the maximum i_d current ($i_q = 0$). (**a**) One magnetic pole 100% demagnetized. (**b**) Two adjacent north magnetic poles 50% demagnetized. (**c**) Two adjacent north-south magnetic poles 50% demagnetized. (**d**) Two adjacent north magnetic poles 100% demagnetized. (**e**) Two adjacent north-south magnetic poles 100% demagnetized. (**f**) Two magnets of the same pole 100% demagnetized. (**g**) Only one magnet 100% demagnetized.

- **Case 1**. One magnetic pole 100% demagnetized. This case corresponds to 1/12 demagnetized magnets, i.e., 8.3% demagnetization.
- **Case 2.** Two adjacent north magnetic poles 50% demagnetized. This case corresponds to 8.3% demagnetization.
- **Case 3.** Two adjacent north-south magnetic poles 50% demagnetized. This case corresponds to 8.3% demagnetization.
- **Case 4.** Two adjacent north magnetic poles 100% demagnetized. This case corresponds to 16.7% demagnetization.
- **Case 5.** Two adjacent north-south magnetic poles 100% demagnetized. This case corresponds to 16.7% demagnetization.
- **Case 6.** Two magnets of the same pole 100% demagnetized. This case corresponds to 7.4% demagnetization.
- **Case 7.** Only one magnet 100% demagnetized. This case corresponds to 5.0% demagnetization.

It is noted that this paper deals with low levels of demagnetization. Whereas cases 1, 2 and 3 correspond to a demagnetization level of 8.3%, cases 4 and 5 correspond to 16.7%.

Partial demagnetization faults are more difficult to detect in fPMa-SynRMs than in other machine types such as surface permanent magnet synchronous motors, due to the lower influence of the permanent magnets on the overall performance of the machine. The analyzed machine presents 56.86% reluctant torque versus 43.14% alignment torque.

4. Results Under Healthy and Partial Demagnetization

This section compares the results attained with the healthy machine and the five partial demagnetization cases described in Section 3. It is worth noting that the harmonic content of the analyzed signals is extracted by applying the FFT.

Tables 2–4 summarize the results attained by means of FEA simulations for the five selected demagnetization cases.

Table 3. Harmonic content of the line currents underrated speed and applying the maximum i_d current ($i_q = 0$). Healthy and partially demagnetized fPMa-SynRMs.

Harmonic Order	1	2	3	4	5	6	7	8	9
Case 1. One magnetic pole 100% demagnetized. Maximum i_d current									
Healthy (A)	**5.01**	-	2.54	-	3.25×10^{-3}	-	0.91	-	0.15
Demagnetized (A)	**4.90**	1.6×10^{-3}	2.49	3.83×10^{-4}	1.40×10^{-4}	6.22×10^{-4}	0.84	1.77×10^{-4}	0.14
Case 2. Two adjacent north magnetic poles 50% demagnetized. Maximum i_d current									
Healthy (A)	**5.01**	-	2.54	-	3.25×10^{-3}	-	0.91	-	0.15
Demagnetized (A)	**4.84**	0.11	2.46	0.03	0.01	0.05	0.54	0.01	0.15
Case 3. Two adjacent north-south magnetic poles 50% demagnetized. Maximum i_d current									
Healthy (A)	**5.01**	-	2.54	-	3.25×10^{-3}	-	0.91	-	0.15
Demagnetized (A)	**4.84**	0.03	2.46	7.57×10^{-3}	3.43×10^{-3}	0.01	0.84	3.17×10^{-3}	0.14
Case 4. Two adjacent north magnetic poles 100% demagnetized. Maximum i_d current									
Healthy (A)	**5.01**	-	2.54	-	3.25×10^{-3}	-	0.91	-	0.15
Demagnetized (A)	**4.80**	0.01	2.45	2.24×10^{-3}	1.02×10^{-3}	3.53×10^{-3}	0.81	1.09×10^{-3}	0.14
Case 5. Two adjacent north-south magnetic poles 100% demagnetized. Maximum i_d current									
Healthy (A)	**5.01**	-	2.54	-	3.25×10^{-3}	-	0.91	-	0.15
Demagnetized (A)	**4.79**	9.50×10^{-3}	2.39	2.33×10^{-3}	1.06×10^{-3}	3.40×10^{-3}	0.75	9.96×10^{-4}	0.12
Case 6. Two magnets of the same pole 100% demagnetized									
Healthy (A)	**5.01**	-	2.54	-	3.25×10^{-3}	-	0.91	-	0.15
Demagnetized (A)	**4.89**	0.07	2.50	0.02	8.23×10^{-3}	0.03	0.85	7.60×10^{-3}	0.14
Case 7. One magnet 100% demagnetized									
Healthy (A)	**5.01**	-	2.54	-	3.25×10^{-3}	-	0.91	-	0.15
Demagnetized (A)	**4.89**	0.04	2.50	9.10×10^{-3}	4.24×10^{-3}	0.01	0.88	3.60×10^{-3}	0.14

Bold numbers indicate the most discriminating harmonics.

Table 4. Harmonic content of the ZSVC underrated speed and applying the maximum i_d current ($i_q = 0$). Healthy and partially demagnetized fPMa-SynRMs.

Harmonic Order	1	2	3	4	5	6	7	8	9
Case 1. One magnetic pole 100% demagnetized. Maximum i_d current									
Healthy (V)	**26.71**	-	**2.52**	-	0.40	-	0.39	-	0.46
Demagnetized (V)	**26.39**	3.47×10^{-3}	**2.09**	1.00×10^{-3}	0.50	7.01×10^{-4}	0.22	5.94×10^{-4}	0.45
Case 2. Two adjacent north magnetic poles 50% demagnetized. Maximum i_d current									
Healthy (V)	**26.71**	-	**2.52**	-	0.40	-	0.39	-	0.46
Demagnetized (V)	**26.28**	0.03	**2.03**	0.02	0.46	0.01	0.65	0.02	0.48
Case 3. Two adjacent north-south magnetic poles 50% demagnetized. Maximum i_d current									
Healthy (V)	**26.71**	-	**2.52**	-	0.40	-	0.39	-	0.46
Demagnetized (V)	**26.10**	4.00×10^{-3}	**2.14**	0.01	0.45	6.38×10^{-3}	0.33	5.65×10^{-3}	0.32
Case 4. Two adjacent north magnetic poles 100% demagnetized. Maximum i_d current									
Healthy (V)	**26.71**	-	**2.52**	-	0.40	-	0.39	-	0.46
Demagnetized (V)	**26.10**	2.02×10^{-3}	**1.56**	1.58×10^{-3}	0.67	1.18×10^{-3}	0.37	1.60×10^{-3}	0.39
Case 5. Two adjacent north-south magnetic poles 100% demagnetized. Maximum i_d current									
Healthy (V)	**26.71**	-	**2.52**	-	0.40	-	0.39	-	0.46
Demagnetized (V)	**25.14**	1.13×10^{-3}	**2.18**	3.73×10^{-3}	0.45	2.24×10^{-3}	0.37	2.67×10^{-3}	0.37
Case 6. Two magnets of the same pole 100% demagnetized									
Healthy (V)	**26.71**	-	**2.52**	-	0.40	-	0.39	-	0.46
Demagnetized (V)	**26.41**	0.03	**2.09**	0.02	0.49	0.02	0.27	0.01	0.45
Case 7. One magnet pole 100% demagnetized									
Healthy (V)	**26.71**	-	**2.52**	-	0.40	-	0.39	-	0.46
Demagnetized (V)	**26.59**	0.02	**2.09**	0.02	0.49	0.01	0.29	0.01	0.46

Bold numbers indicate the most discriminating harmonics.

Table 2 summarizes the harmonic content of the EMF for the five demagnetization cases when the machine rotates at its rated speed.

Results shown in Table 2 clearly show that in all five analyzed partial demagnetization cases it is possible to diagnose the fault condition by analyzing the spectral content of the EMF, the most discriminating harmonics being the first, third and ninth (although the amplitudes of all EMF harmonic components tend to decrease when analyzing partially demagnetized machines.

Table 3 summarizes the results attained when analyzing the changes in the spectral content of the line currents underrated speed and applying the maximum i_d current ($i_q = 0$).

Results presented in Table 3 probe a lower sensitivity of the diagnosis based on the analysis of the stator currents compared to the diagnosis based on the analysis of the EMF. In this case the most discriminating harmonic of the line currents is the first.

Table 4 presents the results obtained when analyzing the changes in the spectral content of the ZSVC underrated speed and applying the maximum i_d current ($i_q = 0$).

Results summarized in Table 4 show that the most discriminating harmonics of the ZSVC are the first and third.

Figure 6 compare the spectral content of the back-EMF and the ZSVC (the most sensitive methods) of a healthy and a partially demagnetized machine when two adjacent north poles are demagnetized 100% each.

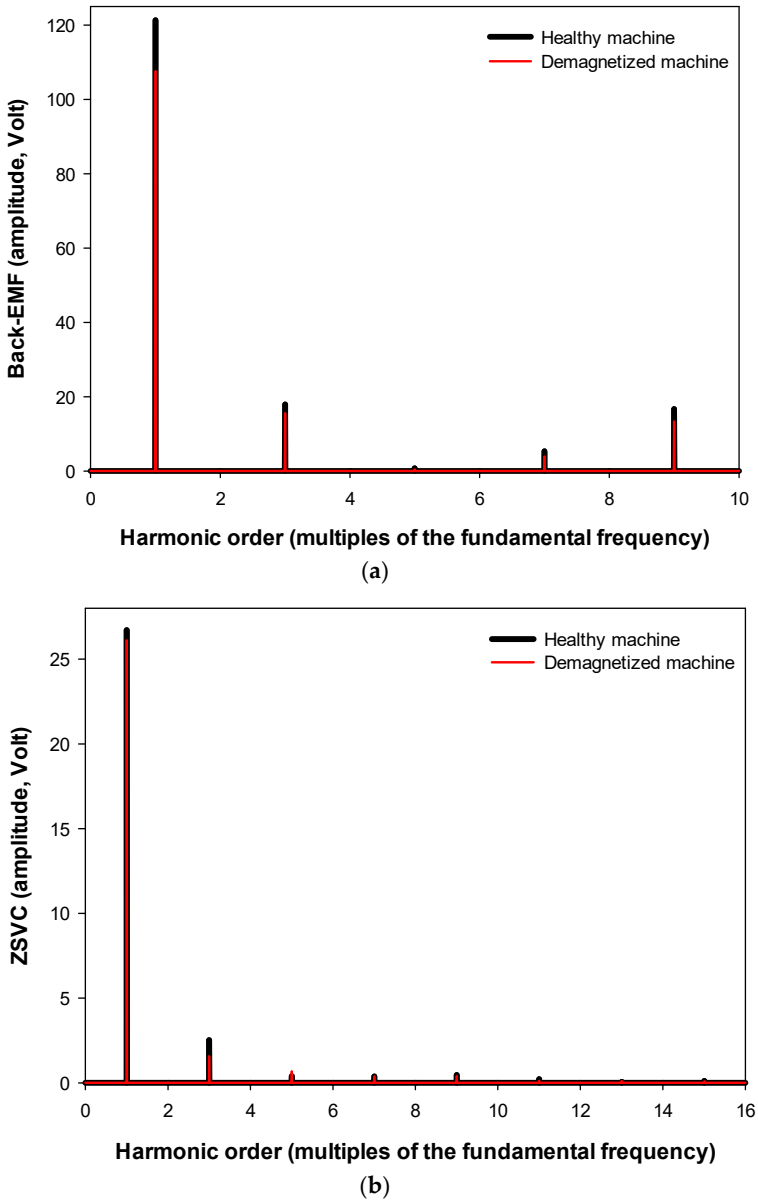

Figure 6. Back-EMF (**a**) and ZSVC (**b**) spectra of a healthy and a partially demagnetized machine (two adjacent north magnetic poles 100% demagnetized).

Finally, Table 5 shows the change in the power factor due to the demagnetization faults underrated speed and applying the maximum i_d current ($i_q = 0$).

Table 5. Power factor underrated speed and applying the maximum i_d current ($i_q = 0$). Healthy and partially demagnetized fPMa-SynRMs.

Harmonic Order	PF
Case 1. One magnetic pole 100% demagnetized. Maximum i_d current	
Healthy (V)	0.47
Demagnetized (V)	0.40
Case 2. Two adjacent north magnetic poles 50% demagnetized. Maximum i_d current	
Healthy (V)	0.47
Demagnetized (V)	0.36

Table 5. *Cont.*

Harmonic Order	PF
Case 3. Two adjacent north-south magnetic poles 50% demagnetized. Maximum i_d current	
Healthy (V)	0.47
Demagnetized (V)	0.41
Case 4. Two adjacent north magnetic poles 100% demagnetized. Maximum i_d current	
Healthy (V)	0.47
Demagnetized (V)	0.36
Case 5. Two adjacent north-south magnetic poles 100% demagnetized. Maximum i_d current	
Healthy (V)	0.47
Demagnetized (V)	0.34
Case 6. Two magnets of the same pole 100% demagnetized	
Healthy (V)	0.47
Demagnetized (V)	0.41
Case 7. One magnet 100% demagnetized	
Healthy (V)	0.47
Demagnetized (V)	0.44

Results presented in Table 5 probe that the PF can be a reliable and simple fault indicator to diagnose low demagnetization levels in PMa-SynRMs, since it is known that the addition of PMs in the rotor increases the PF, and thus, any demagnetization fault is traduced in a reduction of this parameter.

5. Fault Indicators to Detect Demagnetization Faults

Section 4 has evaluated the effect of demagnetization faults on the value of several machine parameters, such as the EMF, the spectral content of the stator currents and the ZSVC, and on the PF. From these results, it is required to calculate suitable fault indicators to diagnose such faults in their early stage. The strategy to follow for calculating such fault indicators and to diagnose the partial demagnetization faults is summarized in Figure 7.

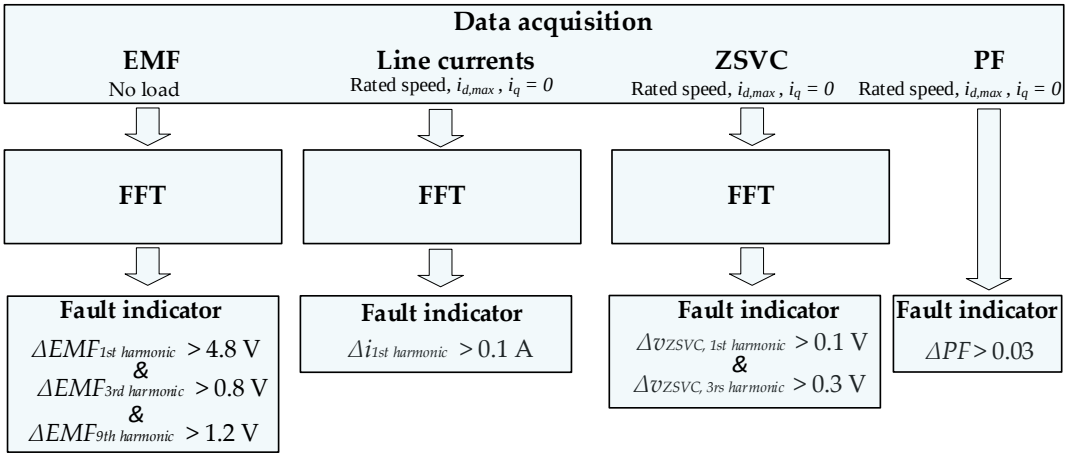

Where:

$$\Delta EMF_{xth\ harmonic} = |EMF_{xth,harmonic,healthy} - EMF_{xth,harmonic,analyzed}|$$
$$\Delta i_{1st\ harmonic} = |i_{1st,harmonic,healthy} - i_{1st,harmonic,analyzed}|$$
$$\Delta v_{ZSVC,\ xth\ harmonic} = |v_{ZSVC\ xth,harmonic,\ healthy} - v_{ZSVC\ xth,harmonic,analyzed}|$$
$$\Delta PF = |PF_{,healthy} - PF_{,analyzed}|$$

Figure 7. Proposed fault indicators and partial demagnetization diagnosis strategy.

The fault indicators described in Figure 7 can be applied separately or in combination to diagnose partial demagnetization faults. They are based on the difference between the magnitudes obtained with the reference healthy condition of the studied machine and the analyzed status of the machine.

According to Figure 7, which also summarizes the results presented in Section 4, the most sensitive methods to detect low level demagnetization faults are, in this order, the analysis of the EMF, ZSVC, PF and, finally, the least sensitive is the analysis of the line currents. The threshold values of the fault indicators shown in Figure 7 have been set to diagnose partial demagnetization faults with a demagnetization level as low as 5.0%. However, these threshold values can be increased according to the values shown in Tables 2–5 for increased levels of demagnetization to be diagnosed.

It is noted that the EMF, line currents, ZSVC and PF can be acquired in real-time with suitable voltage and current sensors. The calculation of the fast FFT to extract the harmonic content of the signals is very fast, requiring some milliseconds in standard computers. Therefore, the proposed fault detection method can be applied on-line.

6. Conclusions

Partial demagnetization faults degrade the performance of PMa-SynRMs, thus affecting the performance and safe operation of the machine. Despite the importance and impact of these faults, there are no published papers dealing with the detection of demagnetization faults in PMa-SynRMs. This paper has proposed and validated different methods to detect partial demagnetization faults in five-phase ferrite PMa-SynRMs, and has developed several fault indicators for this purpose. The methods presented are based on the analysis of the spectral content of the EMF, the spectral content of the line currents, the spectral content of the ZSVC and the analysis of the PF. It has been verified that the most sensitive methods to detect low level demagnetization faults are, in this order, the analysis of the EMF, ZSVC, PF and, finally, the least sensitive is the analysis of the line currents. Results presented in this paper prove the feasibility to detect early demagnetization faults by applying an on-line approach, since demagnetization levels between 5.0% and 16.7% have been analyzed by means of an on-line acquisition of different electrical signals. This is of special relevance since fPMa-SynRMs can be easily demagnetized, whereas low demagnetization levels are more difficult to detect in fPMa-SynRMs than in other machine types, due to the lower impact of the permanent magnets on the overall performance of the machine; thus, this is a challenging problem. The early detection of PM faults allows ensuring that the machine operates under stable and safe conditions, thus avoiding harmful situations. These results may be useful to generate on-line fault diagnosis methods for multi-phase fPMa-SynRMs, which can be used in diverse applications, including the automotive and electromobility sectors.

Author Contributions: J.-R.R. and C.C.-Z. designed and conceived the experiments; C.C.-Z. and D.V.T. performed the experiments; A.G. and J.-R.R. analyzed the data; J.-R.R. wrote the paper. All authors have read and agreed to the published version of the manuscript.

Funding: This research and the APC were funded in part by the Generalitat de Catalunya under grant numbers 2018DI004 and 2017SGR0967.

Conflicts of Interest: The authors declare no conflict of interest.

Nomenclature

$\boldsymbol{i_{a,b,c,d,e}}$	Phase currents (A)
i_d	d-axis current (A)
i_q	q-axis current (A)
$v_{a,b,c,d,e}$	Phase voltage (V)
v_{ZSVC}	Homopolar voltage (V)
f_s	Electrical frequency (Hz)

p	Pole pairs (-)
$R_{a,b,c,d,e}$	Phase resistance (Ω)
L_d	d-axis inductance (H)
L_q	q-axis inductance (H)
θ	Rotor position (electrical °)
α	Current angle (electrical °)
EMF	Electromotive force
FEA	Finite element analysis
FFT	Fast Fourier transform
fPMa-SynRM	Ferrite-assisted synchronous reluctance motor
MCSA	Motor current signature analysis
PF	Power factor
PM	Permanent magnet
PMa-SynRM	Permanent magnet assisted synchronous reluctance motor
ZSVC	Zero-sequence voltage component

References

1. Ngo, D.K.; Hsieh, M.F. Performance Analysis of Synchronous Reluctance Motor with Limited Amount of Permanent Magnet. *Energies* **2019**, *12*, 3504. [CrossRef]
2. Riba, J.-R.; López-Torres, C.; Romeral, L.; Garcia, A. Rare-earth-free propulsion motors for electric vehicles: A technology review. *Renew. Sustain. Energy Rev.* **2016**, *57*, 367–379. [CrossRef]
3. Mahmoud, H.; Bianchi, N. Eccentricity in synchronous reluctance motors—Part I: Analytical and finite-element models. *IEEE Trans. Energy Convers.* **2015**, *30*, 745–753. [CrossRef]
4. Zhu, X.; Wu, W.; Quan, L.; Xiang, Z.; Gu, W. Design and multi-objective stratified optimization of a less-rare-earth hybrid permanent magnets motor with high torque density and low cost. *IEEE Trans. Energy Convers.* **2018**, *34*, 1178–1189. [CrossRef]
5. Ibrahim, M.; Pillay, P. Aligning the Reluctance and Magnet Torque in Permanent Magnet Synchronous Motors for Improved Performance. In Proceedings of the 2018 IEEE Energy Conversion Congress and Exposition, ECCE, Portland, OR, USA, 23–27 September 2018; Institute of Electrical and Electronics Engineers Inc.: Piscataway, NJ, USA, 2018; pp. 2286–2291.
6. Hayslett, S.; Strangas, E. Design and analysis of aligned axis interior permanent magnet machines considering saturation. In Proceedings of the 2019 IEEE International Electric Machines and Drives Conference, IEMDC, San Diego, CA, USA, 12–15 May 2019; Institute of Electrical and Electronics Engineers Inc.: Piscataway, NJ, USA, 2019; pp. 686–692.
7. López-Torres, C.; Riba, J.-R.; Garcia, A.; Romeral, L. Detection of eccentricity faults in five-phase ferrite-PM assisted synchronous reluctance machines. *Appl. Sci.* **2017**, *7*, 565. [CrossRef]
8. Vagati, A.; Boazzo, B.; Guglielmi, P.; Pellegrino, G. Design of ferrite-assisted synchronous reluctance machines robust toward demagnetization. *IEEE Trans. Ind. Appl.* **2014**, *50*, 1768–1779. [CrossRef]
9. Zhu, M.; Yang, B.; Hu, W.; Feng, G.; Kar, N.C. Vold-Kalman Filtering Order Tracking Based Rotor Demagnetization Detection in PMSM. *IEEE Trans. Ind. Appl.* **2019**, *55*, 5768–5778. [CrossRef]
10. Gao, C.; Nie, Y.; Si, J.; Fu, Z.; Feng, H. Mode Recognition and Fault Positioning of Permanent Magnet Demagnetization for PMSM. *Energies* **2019**, *12*, 1644. [CrossRef]
11. Urresty, J.C.J.-C.; Riba, J.R.J.-R.; Romeral, L. Diagnosis of interturn faults in pmsms operating under nonstationary conditions by applying order tracking filtering. *IEEE Trans. Power Electron.* **2013**, *28*, 507–515. [CrossRef]
12. Romary, R.; Demian, C.; Schlupp, P.; Roger, J.-Y. Offline and online methods for stator core fault detection in large generators. *IEEE Trans. Ind. Electron.* **2013**, *60*, 4084–4092. [CrossRef]
13. Candelo-Zuluaga, C.; Riba, J.-R.; López-Torres, C.; Garcia, A. Detection of Inter-Turn Faults in Multi-Phase Ferrite-PM Assisted Synchronous Reluctance Machines. *Energies* **2019**, *12*, 2733. [CrossRef]
14. Faiz, J.; Mazaheri-Tehrani, E. Demagnetization modeling and fault diagnosing techniques in permanent magnet machines under stationary and nonstationary conditions: An overview. *IEEE Trans. Ind. Appl.* **2017**, *53*, 2772–2785. [CrossRef]

15. Cusido, J.; Romeral, L.; Ortega, J.A.; Garcia, A.; Riba, J.R. Wavelet and PDD as fault detection techniques. *Electr. Power Syst. Res.* **2010**, *80*, 915–924. [CrossRef]
16. Huang, B.; Feng, G.; Tang, X.; Gu, J.X.; Xu, G.; Cattley, R.; Gu, F.; Ball, A.D.; Huang, B.; Feng, G.; et al. A performance evaluation of two bispectrum analysis methods applied to electrical current signals for monitoring induction motor-driven systems. *Energies* **2019**, *12*, 1438. [CrossRef]
17. Ilamparithi, T.; Nandi, S. Analysis, modeling and simulation of static eccentric reluctance synchronous motor. In Proceedings of the 8th IEEE Symposium on Diagnostics for Electrical Machines, Power Electronics & Drives, Bologna, Italy, 5–8 September 2011; pp. 45–50.
18. Giantomassi, A.; Ferracuti, F.; Iarlori, S.; Ippoliti, G.; Longhi, S. Electric Motor Fault Detection and Diagnosis by Kernel Density Estimation and KKullback—Leibler Divergence Based on Stator Current Measurements. *IEEE Trans. Ind. Electron.* **2015**, *62*, 1770–1780. [CrossRef]
19. Choi, S.; Haque, M.S.; Arafat, A.; Toliyat, H. Detection and estimation of extremely small fault signature by utilizing multiple current sensor signals in multiphase electric machines. *IEEE Trans. Ind. Appl.* **2017**, *53*, 2805–2816. [CrossRef]
20. Saavedra, H.; Urresty, J.-C.; Riba, J.-R.; Romeral, L. Detection of interturn faults in PMSMs with different winding configurations. *Energy Convers. Manag.* **2014**, *79*, 534–542. [CrossRef]
21. Urresty, J.C.; Riba, J.R.; Delgado, M.; Romeral, L. Detection of demagnetization faults in surface-mounted permanent magnet synchronous motors by means of the zero-sequence voltage component. *IEEE Trans. Energy Convers.* **2012**, *27*, 42–51. [CrossRef]
22. Lee, S.B.; Hyun, D.; Kang, T.; Yang, C.; Shin, S.; Kim, H.; Park, S.; Kong, T.-S.; Kim, H.-D. Identification of false rotor fault indications produced by online mcsa for medium-voltage induction machines. *IEEE Trans. Ind. Appl.* **2016**, *52*, 729–739. [CrossRef]
23. Saavedra, H.; Riba, J.-R.; Romeral, L. Detection of inter-turn faults in five-phase permanent magnet synchronous motors. *Adv. Electr. Comput. Eng.* **2014**, *14*, 49–54. [CrossRef]
24. Urresty, J.-C.; Riba, J.-R.; Romeral, L. Influence of the stator windings configuration in the currents and zero-sequence voltage harmonics in permanent magnet synchronous motors with demagnetization faults. *IEEE Trans. Magn.* **2013**, *49*, 4885–4893. [CrossRef]
25. Vartanian, R.; Toliyat, H.A.; Akin, B.; Poley, R. Power factor improvement of synchronous reluctance motors (SynRM) using permanent magnets for drive size reduction. In Proceedings of the Conference Proceedings-IEEE Applied Power Electronics Conference and Exposition—APEC, Orlando, FL, USA, 5–9 February 2012; pp. 628–633.
26. Faiz, J.; Jafari, A. Interturn fault diagnosis in brushless direct current motors—A review. In Proceedings of the 2018 IEEE International Conference on Industrial Technology (ICIT), IEEE, Lyon, France, 20–22 February 2018; pp. 437–444.
27. Ullah, Z.; Hur, J. A comprehensive review of winding short circuit fault and irreversible demagnetization fault detection in PM type machines. *Energies* **2018**, *11*, 3309. [CrossRef]
28. Schramberg Hard Ferrite Magnets. Strontium Ferrite HF 30/26. Available online: https://www.magnete.de/fileadmin/user_upload/Content/Produkte/PDF/Gesinterte_HF_Magnete/HF_30-26_E.pdf (accessed on 15 June 2020).